Nonlinear Reduced-Order Analysis with Time-Varying Spatial Loading Distributions

Adam Przekop[1]
National Institute of Aerospace, Hampton, VA 23666

and

Stephen A. Rizzi[2]
NASA Langley Research Center, Hampton, VA 23681

Oscillating shocks acting in combination with high-intensity acoustic loadings present a challenge to the design of resilient hypersonic flight vehicle structures. This paper addresses some features of this loading condition and certain aspects of a nonlinear reduced-order analysis with emphasis on system identification leading to formation of a robust modal basis. The nonlinear dynamic response of a composite structure subject to the simultaneous action of locally strong oscillating pressure gradients and high-intensity acoustic loadings is considered. The reduced-order analysis used in this work has been previously demonstrated to be both computationally efficient and accurate for time-invariant spatial loading distributions, provided that an appropriate modal basis is used. The challenge of the present study is to identify a suitable basis for loadings with time-varying spatial distributions. Using a proper orthogonal decomposition and modal expansion, it is shown that such a basis can be developed. The basis is made more robust by incrementally expanding it to account for changes in the location, frequency and span of the oscillating pressure gradient.

Nomenclature

a	=	quadratic modal stiffness coefficient
b	=	cubic modal stiffness coefficient
$[C],[\tilde{C}]$	=	physical degree-of-freedom damping matrix, modal damping matrix
d	=	linear modal stiffness coefficient
$\{f\},\{\tilde{f}\}$	=	physical degree-of-freedom force vector, modal force vector
$\{f_{NL}\},\{\tilde{f}_{NL}\}$	=	physical degree-of-freedom restoring force vector, modal restoring force vector
$[\Phi],\{\phi\}$	=	matrix of normal modes, normal mode vector
$[I]$	=	identity matrix
L	=	number of modal basis functions
$[\lambda]$	=	proper orthogonal value matrix
m	=	number of nodes in finite element model
M	=	number of most contributing proper orthogonal modes
$[M],[\tilde{M}]$	=	physical degree-of-freedom mass matrix, modal mass matrix
n	=	number of displacement fields used in snapshot matrix
N	=	number of physical degrees-of-freedom
$[P],\{p\}$	=	matrix of proper orthogonal modes, proper orthogonal mode vector
q	=	modal (generalized) coordinate
$[R]$	=	correlation matrix

[1] Research Scientist, c/o NASA Langley Research Center, MS 463, Hampton, VA 23681, AIAA Senior Member.
[2] Aerospace Engineer, Structural Acoustics Branch, NASA Langley Research Center, MS 463, Hampton, VA 23681, AIAA Associate Fellow.

$[S],\{s\}$	=	matrix of modal expansion coefficients, vector of modal expansion coefficients
t	=	time
υ	=	cumulative proper orthogonal mode participation factor
$[X],\{x\}$	=	displacement snapshot matrix, displacement time history vector
χ_i	=	i^{th} proper orthogonal mode participation factor
ζ	=	viscous damping factor
ω	=	undamped natural frequency

I. Introduction

DESPITE the fact that commercial off-the-shelf finite element (FE) tools exist for time domain analysis of strongly nonlinear response regimes, the computational expense associated with their application is often prohibitive. Consequently, a nonlinear modal transformation from the analysis in physical degrees-of-freedom (DoFs) to one in modal coordinates is sought to reduce the system size. Over the years, time domain FE-based nonlinear reduced-order simulation methods have been extensively developed for application to a diverse spectrum of dynamic response problems.[1] Cases with time-varying loading distributions, however, have received little attention. Moreover, reduced-order systems have been usually formed for specific loading conditions and response regimes, such that a perturbed operating condition required re-development of a different reduced-order system. In such cases, the difficulty in developing more robust nonlinear reduced-order basis stemmed from the fact that the desired modal basis was changing with time.

The present work expands the application of a recently developed procedure for modal basis selection[2,3] to the analysis of problems with time-varying special loading distributions. The procedure is based on system identification via proper orthogonal decomposition (POD).[4,5] The proper orthogonal modes (POMs), however, change with loading distribution and intensity, so they do not constitute an efficient basis. Therefore, an additional step involving modal expansion seeks to identify normal modes (NMs) resembling POMs. In the past, a basis formed using NMs was found to be applicable over a broad range of response regimes having a fixed loading distribution.[2,3] In the present study, a basis that is also applicable over a perturbed set of spatially time-varying loading conditions is sought. By repeating the basis selection procedure, new NM bases may be found for perturbations of the spatially time-varying loading condition. Finally, because all the NMs are orthogonal, these bases may be combined to form a single NM basis applicable over the range of loading conditions analyzed. In doing so, a significant computational savings may be achieved.

To demonstrate that the proposed approach is applicable to time-varying spatial loading distributions, the focus of the present work is on a structure simultaneously subjected to an oscillating pressure gradient and high-intensity acoustic loading. This condition was motivated by oscillating shocks acting in combined thermal-acoustic loading environments, as encountered on hypersonic flight vehicle structures.[6] Figure 1 depicts such a loading case in which an oscillating shock formed ahead of a compression ramp[7,8] combines with an acoustic disturbance generated by a scram jet propulsion system.[6] In such a scenario, the acoustic disturbance will forward propagate only in the subsonic region aft of the shock. The effects of fluid and thermal loadings, while significant in the motivational problem, are not included in this study. The loading conditions considered are presented in Figure 2. The structure is modeled as a composite plate strip and the strength of the pressure gradient and oscillation frequency were guided by available empirical data.[7,8] The reference condition is indicated as load case 1 in Table 1, while perturbations of selected parameters including location, frequency and span of the oscillating pressure gradient are indicated as load cases 2-7.

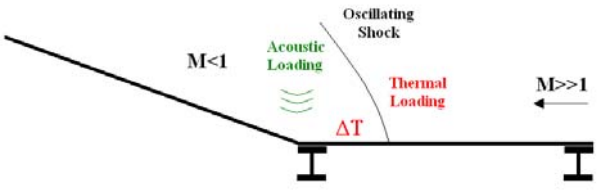

Figure 1: Oscillating shock due to hypersonic flow over compression ramp.

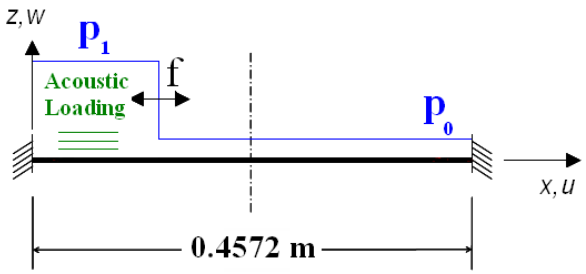

Figure 2: Composite plate strip under simplified time-varying spatial loading distribution.

Table 1: Time-varying spatial loading distributions.

Load Case	Oscillation Span (m)	Oscillation Center Position *x* (m)	Oscillation Frequency (Hz)	Max. Oscillation Speed (m/s)
1	0.0127	0.1143	714	28.49
2	0.0127	0.0572	714	28.49
3	0.0127	0.1715	714	28.49
4	0.0635	0.1143	142.8	28.49
5	0.1270	0.1143	7.14	2.849
6	0.1270	0.1143	71.4	28.49
7	0.1270	0.1143	714	284.9

II. Formulation

The system identification employed by the authors[3] is next reviewed and a modal basis selection criterion employing a modal expansion approach[2] is summarized. The previously developed modal system reduction by an indirect nonlinear stiffness evaluation procedure[9,10] is also briefly discussed.

A. System Identification – Proper Orthogonal Decomposition

When physical DoFs are chosen to characterize the response, a snapshot matrix $[X]$ can be formed as an accumulation of n instantaneous displacement, velocity, or acceleration response fields.[4,5] In the current analysis, displacement fields obtained from a nonlinear FE analysis are used resulting in a snapshot matrix of size $n \times N$, where N is the number of DoFs. The sample rate and spatial resolution of the snapshot matrix must be sufficient to resolve the system's temporal and spatial characteristics of interest. The correlation matrix $[R]$, of size $N \times N$, is formed as

$$[R] = \frac{1}{n}[X]^T [X]. \tag{1}$$

An eigenanalysis of the correlation matrix is next performed, i.e,

$$\left([R] - [\lambda][I]\right)\{y\} = \{0\} \tag{2}$$

to obtain a POM matrix $[P] = \left[\{p_1\}\ \{p_2\} \ldots \{p_N\}\right]$ and the diagonal proper orthogonal value (POV) matrix, $[\lambda]$, both of size $N \times N$. Each POV is a measure of the corresponding POM activity, i.e., the higher the POV, the greater the contribution of a corresponding POM to the dynamic response.

The POD procedure employed is performed independently for each DoF type of interest by partitioning the snapshot matrix. In the subsequent POD analyses, three out of six available DoF types for shell FEs are considered, i.e., transverse displacement w and two in-plane displacements u and v. The two out-of-plane rotations, ϕ_x and ϕ_y, were previously found[2] to ultimately yield the same set of NMs as the transverse displacement DoF, so they are not considered in the present analysis. The sixth DoF type, the rotation about the normal to the plate surface ϕ_z, also called the drilling DoF, also is not considered since it is not common to all shell element formulations. By adopting this approach, the size of each individual DoF snapshot matrix $[X]$ is reduced to $n \times m$, where m is the number of nodes, and the size of each individual correlation matrix $[R]$, POM matrix $[P]$, and POV matrix $[\lambda]$ is reduced to $m \times m$.

B. Modal Basis Selection

The contribution of each POM to the overall dynamic response is given by

$$\chi_i = \lambda_i \Big/ \sum_{j=1}^{m} \lambda_j \qquad i = 1, \ldots, m \tag{3}$$

where χ_i is the i^{th} POM participation factor. The sum of all POM participation factors is unity. When the most contributing M POMs are selected, their cumulative participation, υ, can be expressed as

$$\upsilon = \sum_{i=1}^{M} \chi_i \qquad 0 < \upsilon \le 1 \ . \tag{4}$$

Retention of only the selected M POMs reduces the size of $[P]$ to m x M.

As previously indicated, the direct use of POMs for the basis is not preferred for a forced response problem as they are load specific. Instead a set of NMs which either directly resemble, or can be superposed to resemble the POMs is sought. The authors recently presented two criteria for identifying such a set using the modal assurance criterion[11] (MAC) and a modal expansion approach.[2] Because of the loading considered, the POMs identified in this work often bore little direct resemblance to NMs. Consequently, the MAC approach was not generally effective and is therefore not considered in this paper.

Modal Expansion Approach

A single POM may be decomposed into a linear superposition of NMs using the expansion[12]

$$\{p_i\} = \sum_{j=1}^{L} c_{ij} \{\phi_j\} \tag{5}$$

where c_{ij} are the expansion coefficients. Since the NMs $\{\phi\}$ are orthogonal, i.e.,

$$\{\phi_k\}^T \{\phi_l\} = \{0\} \qquad k \neq l \tag{6}$$

pre-multiplying Eq. (5) by $\{\phi_k\}^T$ yields

$$s_{ik} = c_{ik} \{\phi_k\}^T \{\phi_k\} = \{\phi_k\}^T \{p_i\} \tag{7}$$

The coefficient matrix $[S]$ may be formed by evaluating Eq. (7) over all selected POMs $(i = 1, ..., M)$ and over all NMs $(k = 1, \ldots, N)$, and may be written in compact form as:

$$[S] = [\Phi]^T [P] \ . \tag{8}$$

One $[S]$ matrix is formed for every DoF type and the size of each $[S]$ matrix is $N \times M$.

Each column of $[S]$ corresponds to a specific POM. Because the POMs $[P]$ used to compute the $[S]$ matrix are not normalized, it is convenient to normalize each column of this matrix to unity so that a single threshold value can be used to identify the most significant NMs. In this work, those modes above a threshold value of 0.5 were included in the basis.

C. Nonlinear Reduced-Order Analysis

Once a set of basis functions consisting of NMs is selected using modal expansion, the nonlinear modal reduction of the system can proceed. A reduced-order method gains its computational advantage by reducing the size of the system in physical DoFs (full-order) to a much smaller system expressed in generalized coordinates (reduced-order). For the problem of interest, the equation of motion in physical DoFs is expressed as

$$[M]\{\ddot{x}(t)\} + [C]\{\dot{x}(t)\} + \{f_{NL}(x(t))\} = \{f(t)\}, \tag{9}$$

where $[M]$ and $[C]$ are the structural mass and damping matrices, and $\{x\}$, $\{f_{NL}\}$, and $\{f\}$ are the physical displacement, nonlinear restoring force, and excitation force vectors, respectively. By applying the modal transformation

$$\{x(t)\} = [\Phi]\{q(t)\}, \tag{10}$$

the reduced-order equation of motion becomes

$$[\tilde{M}]\{\ddot{q}(t)\} + [\tilde{C}]\{\dot{q}(t)\} + \{\tilde{f}_{NL}(q_1(t), q_1(t), \ldots, q_L(t))\} = \{\tilde{f}(t)\} \tag{11}$$

where $\{q\}$ is a generalized coordinate vector and $[\Phi]$ is a matrix containing L selected NMs of the basis. The modal nonlinear restoring force in Eq. (11) can be expressed as

$$\left\{\tilde{f}_{NL}\right\} = [\Phi]^T \{f_{NL}\} \ . \tag{12}$$

Because mass-normalized NMs are used as the basis functions, the modal mass and damping matrices can be expressed as

$$\left[\tilde{M}\right] = [\Phi]^T [M][\Phi] = \lceil I \rfloor \qquad \left[\tilde{C}\right] = [\Phi]^T [C][\Phi] = \lceil 2\zeta_r \omega_r \rfloor , \tag{13}$$

where ω_r and ζ_r are the undamped natural frequencies and the viscous damping factors, respectively. The modal excitation force vector is $\{\tilde{f}(t)\} = [\Phi]^T \{f(t)\}$.

The system reduction utilized in this study is based on the indirect approach employing a nonlinear stiffness evaluation procedure.[9,10] The procedure expresses the r^{th} component of the nonlinear modal restoring force vector as

$$\tilde{f}^r_{\mathrm{NL}}(q_1,\ldots,q_L) = \sum_{j=1}^{L} d^r_j q_j + \sum_{j=1}^{L}\sum_{k=j}^{L} a^r_{jk} q_j q_k + \sum_{j=1}^{L}\sum_{k=j}^{L}\sum_{l=k}^{L} b^r_{jkl} q_j q_k q_l \qquad r = 1,\ldots,L \tag{14}$$

where *d*, *a*, and *b* are the linear, quadratic, and cubic modal stiffness coefficients. Different combinations of scaled NMs form a set of prescribed displacement fields. The normal mode vectors are scaled by the generalized coordinates $\{q\}$ to obtain physically meaningful magnitudes. Using a nonlinear static FE analysis, the nonlinear restoring forces corresponding to each prescribed displacement field are computed in physical DoFs and transformed to the generalized coordinates per Eq. (12). As the vector $\{f_{NL}\}$ and the generalized coordinates $\{q\}$ are known, Eq. (14) constitutes a system of algebraic equations from which the linear, quadratic and cubic modal stiffness coefficients may be determined. The number of unknown coefficients, and hence the number of nonlinear static solutions required for a transformation utilizing L modes is

$$\textit{Number of NL Static Solutions} = 3\binom{L}{1} + 3\binom{L}{2} + \binom{L}{3} \qquad L \geq 3 \tag{15}$$

where

$$\binom{L}{k} = \frac{L!}{k!(L-k)!} \ . \tag{16}$$

Note that the three terms in Eq. (15) reflect the number of linear, quadratic, and cubic modal stiffness coefficients, respectively. The number of nonlinear static solutions can be viewed as a measure of the fixed cost of the reduced-order analysis, as the modal reduction must be performed regardless of the simulated response time to be eventually computed. Once the coefficients have been determined, the Eq. (11) is integrated using a fourth-order Runge-Kutta scheme and the physical displacements recovered through Eq. (10). The reduced-order analysis was implemented in the code RANSTEP[10], which can use either the ABAQUS[13] or MSC.NASTRAN[14] FE codes for NMs analysis, nonlinear static solutions, and stress/strain post-processing.

III. Results

The FE model developed for the ensuing numerical analyses is next presented. The process for generating the time-varying spatial loading distribution follows, with particular attention paid to the high frequency components generated in the region of pressure oscillation. A thorough treatment of a reference load case is then considered to lend insight into the selection of a modal basis using the above approach, and to demonstrate the accuracy of a reduced-order nonlinear simulation vis-à-vis a full-order simulation. Loading parameters are next perturbed to investigate the influence of oscillation position, frequency and span on the response and modal basis selection. Finally, the computational effort associated with a robust, expanded modal basis is addressed.

A. Finite Element Model and Analyses

A composite plate strip clamped at both ends was used as the numerical test article. The structure under investigation, shown in Figure 2, measured 0.4572 x 0.0254 x 0.002 m (*l* x *w* x *h*). Sixteen 0.125 mm layers are stacked in the lamination sequence $(45/0/\text{-}45/90/45/0/\text{-}45/90)_s$. Because the laminate was symmetric, there was no bending/extensional coupling. Material properties for graphite-epoxy lamina were used: Young's modulus E_1 = 181.1 GPa and E_2 = 10.3 GPa, Poison ratio ν_{12} = 0.28, shear modulus $G_{12} = G_{13} = G_{23}$ = 7.17 GPa, mass density ρ =

1550 kg/m^3. The mass proportional damping of C = 11.223 1/s was applied, and the value corresponded to 1.3 % critical damping of the first symmetric transverse mode at f_1 = 68.7 Hz.

A single FE model of the plate strip was constructed for both the full-order and reduced-order analyses. It consisted of 1216 ABAQUS S4R shell elements defined by 1525 nodes for the total of 9150 DoFs. The S4R element has four nodes, each with three translational and three rotational DoFs. All elements used had a width of 6.35 mm, so that four elements spanned the width of the strip. The length of the elements was either 3.125 or 0.635 mm. The smaller element length was used over the greatest region of oscillating pressure loading, i.e. from 50.8 mm to 177.8 mm.

The full-order nonlinear response of the plate strip was analyzed in physical DoFs using the ABAQUS/Explicit solution. Because of the small element size used in the region of pressure oscillation, the automatic "element-by-element" time step adjustment scheme used in ABAQUS yielded an extremely small integration time step of 55.54 x 10^{-9} s. Hence the full-order simulations were computationally very intensive, making only short time simulations feasible. The reduced-order analyses were performed with a much larger integration time step increment of 1.25 x 10^{-6} s.

B. Load Generation

The beam was subjected to a static pressure loading of $P_o = 1$ kPa ahead (to the right) of the lateral pressure oscillation boundary and a static pressure loading of $P_1 = 10$ kPa behind (to the left of) the lateral pressure oscillation boundary, see Figure 2. This pressure rise is on the order of that cited by Elfstrom[8] for a hypersonic M 9.22 flow incident upon a 15° compression wedge. The pressures P_o and P_1 were applied uniformly across the width and the affected length of the strip. The pressure oscillation boundary between P_o and P_1 moved in a sinusoidal fashion, at frequencies indicated in Table 1. In the region of travel, the instantaneous resultant force was calculated and applied proportionally across the nearest element nodes. This representation of the oscillating load was mathematically convenient to implement and was not intended to precisely model an oscillating shock. In addition, a uniformly distributed random acoustic loading of 160 dB overall sound pressure level (ref: 20 μ Pa) over the frequency range 0 – 1024 Hz was applied behind the pressure oscillation boundary. The acoustic pressure tracked left and right with the boundary movement such that no acoustic loading was applied ahead of the boundary.

The pressure time history in the mid-span region of oscillation is shown in Figure 3 for an oscillation span of 63.5 mm and frequency of 142.8 Hz (load case 4). At this location, the oscillation boundary reaches its maximum oscillation speed of 28.49 m/s. The pressure time history is shown both with and without the acoustic loading to demonstrate the modulation induced by the acoustic loading on the 10 kPa static pressure behind the oscillation boundary. The transition between high and low pressure occurs over a short time period of time, such that the resulting pressure time history resembles a square wave. The chopping of the acoustic pressure effectively halves the overall level in the mid-span region of oscillation. Note that at the high static pressure end, the attenuation is minimal, while at the low static pressure end, the gain is minimal. The effect of the pressure oscillation is dramatically shown in its power spectral density (PSD) in Figure 4. Because the waveform is square, spectral peaks are generated at the oscillation frequency and its odd harmonics. The peaks extend to very high frequencies (> 40 kHz). The most noticeable effect is the generation of high frequency broadband noise above the acoustic loading cutoff of 1024 Hz, as shown by the red trace. This distortion occurs as a result of chopping the acoustic loading and, as previously noted, has a secondary effect of reducing the overall acoustic generated component by approximately 3 dB. This is most clearly seen through comparison of the in-band acoustic spectrum with and without the oscillation, shown by the red and black trace, respectively. Although the overall acoustic component is reduced, the combined overall level (broadband acoustic and spectral peaks) is increased by roughly 7 dB to 167 dB, not including the sizeable zero frequency component. This behavior was found to exist for all load cases, each of which had comparable amplification but differing peak behaviors. Because the integrated amplification is the same irrespective of the oscillation frequency, lower oscillation frequencies have lower amplitudes since more harmonics are integrated over the given bandwidth than a higher frequency oscillation. For example, the amplitude of a 7.14 Hz oscillation is lower than that of the 71.4 Hz oscillation.

The net effect of the distorted fluctuating pressure loading on the structural response is twofold. First, spectral peaks, though narrow, have the potential to cause large structural dynamic response if located in the vicinity of a structural resonance. Second, the high frequency content of the loading will excite a greater number of low frequency bending NMs compared to the undistorted acoustic spectrum, and has the potential to directly excite higher frequency in-plane NMs. The anticipated result is that a larger modal basis will be required for the reduced-order analysis.

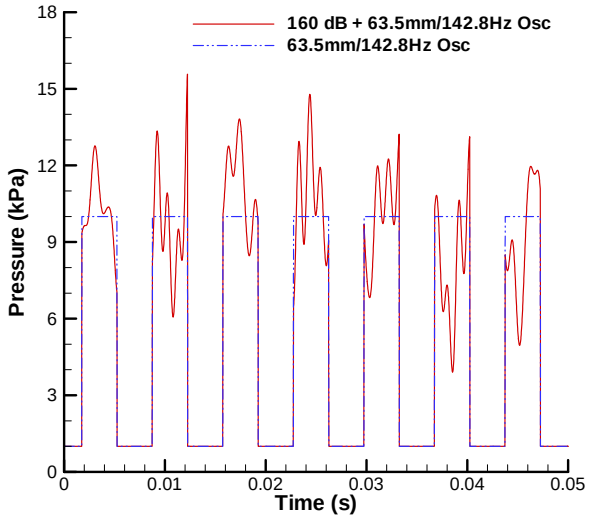

Figure 3: Unsteady pressure time history for load case 4 both with and without the 160 dB acoustic loading.

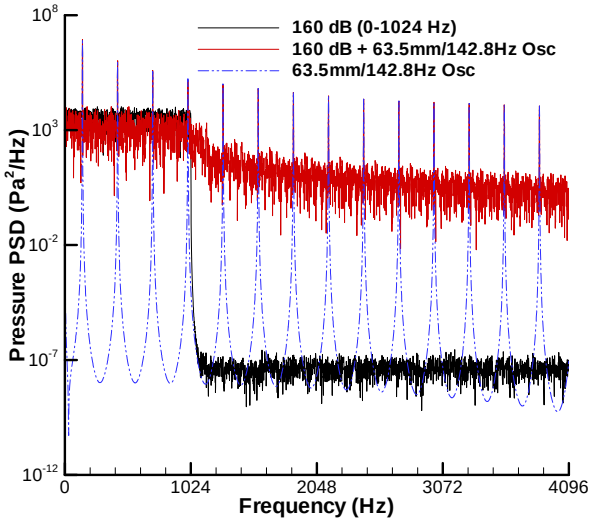

Figure 4: Pressure PSD for load case 4 with and without the 160 dB acoustic loading.

C. Analysis of Reference Condition – Load Case 1

For analysis of the reference condition and perturbed load cases (see Table 1), a single 1.0 s full-order nonlinear response simulation was run with an output interval of 50 μs. In each case, the first 0.5 s of response was removed to minimize the effect of start up transients. Thus, the POD analyses were performed using $n = 10,000$ full-field displacement snapshots. Displacement response PSDs were computed using this data for all load cases except for the reference condition. The full-order simulation was extended by 1.1384 s for the reference condition, giving 1.6384 s of evolved response for computation of the PSD to permit better comparisons with the reduced-order analysis.

Also common to all load cases was the selection of a cumulative POV contribution υ of 99.9 % for the *u* and *v* displacement components, and of 99.999 % for the *w* displacement component. The higher value for the *w* displacement component was selected to help identify additional low frequency bending NMs which lie above the direct acoustic loading bandwidth of 1024 Hz. The contribution of such modes has been previously found to be important[2,3].

The POD analysis for the reference condition identified 29 POMs falling within the cumulative POV contribution values selected. Of these, 14 were associated with the *u* displacement component, 4 with the *v* displacement component, and 11 with the *w* displacement component. A listing of POMs and their individual and cumulative contributions is provided in Table 2. It is seen that the *w* displacement component converges faster than the *u* displacement component for a cumulative POV contribution of 99.9 % (7 POMs for the *w* displacement and 14 POMs for the *u* displacement). This is consistent with earlier work on beam and plate structures subject to uniformly distributed loadings[2,3]. Additionally noteworthy is the result of the NM selection via modal expansion which identified 32 NMs for this load case. There is a nearly 1:1 ratio of POMs to NMs for the *v* and *w* POM displacement components, but generally less so for the *u* POM displacement. This observation, however, does not generally hold for other load cases in which several NMs may be required to superpose to resemble even highly contributing *w* displacement POMs. For brevity, this data is not presented. A list of selected NMs and type (span-wise symmetric or anti-symmetric) is provided in Table 3. NMs in the frequency bandwidth to 100 kHz were considered in this study.

Table 2: POVs and NMs identified for the reference condition (load case 1).

POM Displacement Component	POM Number	POV Contribution (%)	Cumulative POV Contribution (%)	NM # Identified via Modal Expansion
u	1	58.1877	58.187	29, 45
	2	17.2474	75.435	45
	3	11.7966	87.232	6, 237
	4	5.8059	93.038	65
	5	2.9763	96.014	87
	6	1.0584	97.072	105
	7	1.0509	98.123	119, 135
	8	0.7208	98.844	11, 234, 240
	9	0.3130	99.157	148
	10	0.2594	99.416	105, 119, 135, 176
	11	0.2260	99.642	148, 234, 240
	12	0.1431	99.785	198
	13	0.1127	99.898	176, 217
	14	0.0386	99.937	19, 252
v	1	96.9139	96.914	6
	2	2.6627	99.577	11
	3	0.2439	99.820	19
	4	0.1003	99.921	26
w	1	86.4090	86.409	1
	2	6.4862	92.895	3
	3	2.8936	95.789	2
	4	2.5917	98.381	4
	5	1.2016	99.582	5
	6	0.2546	99.837	7
	7	0.1250	99.962	9
	8	0.0253	99.987	8
	9	0.0052	99.992	12, 13
	10	0.0051	99.997	10
	11	0.0013	99.999	14, 15

The PSDs of the quarter-span transverse displacement response computed using full-order and reduced-order nonlinear simulations are presented in Figure 5. This location was chosen to monitor because it lies in the middle of most severe loading. The reduced-order simulation captures both the zero-frequency behavior associated with the static pressure loading and the higher frequency response very well. A non-resonant spectral peak at the 714 Hz oscillation frequency is barely noticeable in this response as the amplitude of the nonlinear frequency response decreases with increasing frequency. An inspection of the response above 1024 Hz indicated similar behavior (not shown). Figure 6 shows the quarter-span in-plane displacement PSD, whose amplitude is about four orders of magnitude lower than that of the transverse response. The reduced-order analysis compares favorably with the full-order analysis across the frequency range. As with the transverse response, the 714 Hz oscillation frequency is barely noticeable.

Table 3: Selected (unstressed) NMs for each load case. NM selections common to all cases are highlighted.

NM # / Type*	Dominant Displacement	Freq. (Hz)	Load Case Number						
			1	2	3	4	5	6	7
1 S	*w*	68.696	+	+	+	+	+	+	+
2 A	*w*	189.29	+	+	+	+	+	+	+
3 S	*w*	371.07	+	+	+	+	+	+	+
4 A	*w*	613.51	+	+	+	+	+	+	+
5 S	*w*	730.85	+		+	+	+	+	+
6 S	*v*	797.03	+	+	+	+	+	+	+
7 S	*w*	916.83	+	+	+	+	+	+	+
8 A	*w*	1281.2	+	+	+	+	+	+	+
9 A	*w*	1465.1	+		+	+	+	+	+
10 S	*w*	1706.7	+	+	+	+	+	+	+
11 A	*v*	2146.6	+	+	+	+	+	+	+
12 A	*w*	2190.1	+		+				+
13 S	*w*	2208.9	+						
14 S	*w*	2740.1	+		+				
15 A	*w*	2957.1	+						
19 S	*v*	4087.0	+	+	+	+	+	+	+
21 A	*w*	4744.3			+				
26 A	*v*	6527.7	+	+	+	+	+	+	+
29 A	*u*	7342.5	+	+	+	+	+	+	+
34 S	*v*	9387.3		+					
41 A	*v*	12,591		+					
45 A	*u*	14,682	+	+	+	+	+	+	+
65 S	*u*	22,015	+	+	+	+	+	+	+
87 A	*u*	29,337	+	+	+	+	+	+	+
105 S	*u*	36,644	+	+	+	+	+	+	+
119 A	*u*	43,930	+	+	+	+	+	+	+
135 S	*u*	51,186	+	+	+	+	+	+	+
148 A	*u*	58,403	+	+	+	+	+	+	+
176 S	*u*	65,566	+	+	+	+	+	+	+
198 A	*u*	72,656	+	+	+	+	+	+	+
217 S	*u*	79,644	+	+					+
234 A	*u*	86,491	+						+
237 S	*u*	86,907	+		+	+	+		+
240 A	*u*	88,131	+		+	+	+	+	+
252 A	*u*	92,499	+	+					
		Total	32	25	28	25	25	24	28

***** S – Span-wise symmetric, A – Span-wise anti-symmetric

From the data presented in Figure 5 and Figure 6, several important conclusions can be made, the most significant of which is that the reduced-order analysis embodied in this work is capable of modeling time-varying spatial loading distributions provided that an adequate basis is used. Secondly, the combination of POD and modal expansion has been shown to be effective for identifying such a basis. Finally, because the loading contains high frequency components and is spatially concentrated, the modal basis is larger than that required for a uniformly distributed loading with lower frequency content. [15]

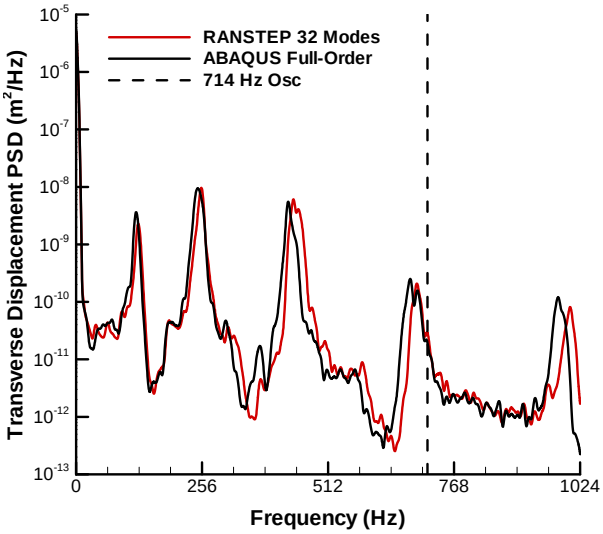

Figure 5: Transverse displacement PSD at quarter-span location for load case 1.

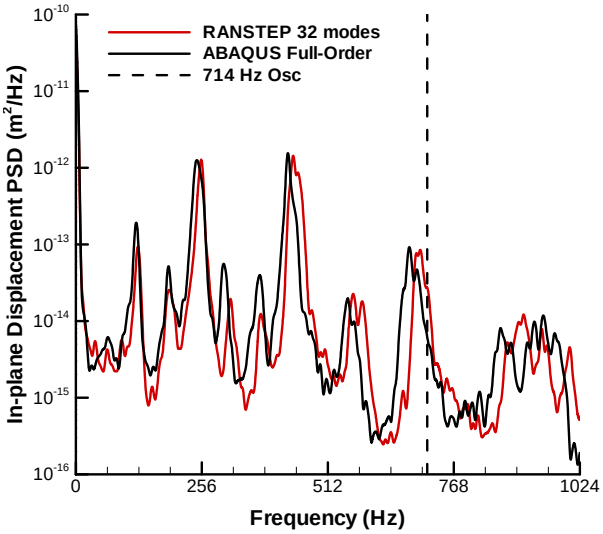

Figure 6: In-plane displacement PSD at the quarter-span location for load case 1.

D. Perturbations of oscillation position, frequency and span

In order to determine the requirements for an expanded basis applicable over perturbed flight conditions, and at the same time gain further insight into the nonlinear structural dynamic response associated with this problem, the effects of varying the oscillation center position, frequency and span were investigated.

Effect of Oscillation Center Position

The effect of the oscillation center position was investigated by perturbing load case 1 such that the center of the oscillation was located nearer to the left clamped end at span-wise location 0.0572 m (load case 2), and nearer to the center at span-wise location 0.1715 m (load case 3), while maintaining an oscillation span of 0.0127 m and oscillation frequency of 714 Hz.

The quarter-span transverse displacement PSDs, shown in Figure 7, were computed using 0.5 s of full-order simulation data. Therefore, they appear less refined than those presented in Figure 5 and Figure 6. Nevertheless, useful conclusions can be drawn from them. Load case 2 has the least amount of exposure to the high amplitude static pressure P_1, consequently the stiffening effect due to application of the static pressure is less than it is for load cases 1 and 3. Therefore, its resonances are only slightly shifted to the higher frequencies, relative to the stressed natural frequencies indicated in Table 3. The area of applied static pressure P_1 increases for load case 1 and is greatest for load case 3, so the frequency shift is progressively greater. Even though the plate strip is stiffest for case 3, followed by case 1, followed by case 2, the amplitude of the response has the opposite trend. It is greatest for case 3, followed by case 1, followed by case 2. This is because the acoustic loading area also increases as the center of oscillation moves from left to right. The response associated with load case 2 appears nearly linear as the strip is exposed to only 0.0572 m of length on average. The 714 Hz oscillation frequency is hardly noticeable in any load case response.

The POD/modal expansion analysis identified 25 NMs associated with 18 POMs for load case 2, and 28 NMs associated with 21 POMs for load case 3. The breakdown of POMs by component type for each load case is shown in Table 4, whilst the particular NMs identified for each case are indicated in Table 3. Load case 1 identified more significant *u* and *w* component POMs than either load case 2 or 3. We surmise this is solely due to the oscillation center position since load case 1 had neither the greatest response nor exhibited the greatest stiffening. Although the oscillation center for load case 1 is collated with the quarter-span monitoring point, this is unrelated to the number of significant POMs as the latter are determined by the global response. The number of *v* component POMs is small and their number appears nearly independent of load case. A general trend seen is that a lower number of POMs usually results in a lower number of NMs being identified.

It should be emphasized that the POMs differ between each load case, i.e., *u* component POM number 1 for load case 1 is different than *u* component POM number 1 for load case 2. The NMs, however, are the same for each

load case as they are determined from the stress-free linear eigenanalysis. The fact that many of the same NMs are represented for differing load cases is why they are desirable for forming the basis.

Table 4: Summary of POMs and NMs for each loading case.

Case	Number of *u* component POMs	Number of *v* component POMs	Number of *w* component POMs	Total Number of –	
				POMs	NMs
1	14	4	11	29	32
2	7	5	6	18	25
3	8	4	9	21	28
4	8	4	9	21	25
5	9	3	8	20	25
6	8	3	8	19	24
7	10	3	10	23	28

Effect of Oscillation Frequency

Next, the oscillation frequency was varied by two orders of magnitude. Load cases 5 (7.14 Hz), 6 (71.4 Hz) and 7 (714 Hz) were considered in order to maintain the same oscillation center position and span. The quarter-span transverse displacement PSDs are shown in Figure 8. As seen in cases 1-3, the 714 Hz oscillation frequency for case 7 is too high to significantly drive the response. The transverse displacement response for load case 6 is significantly driven by the 71.4 Hz oscillation frequency. Additional forced responses at the odd harmonics are less distinguishable. The 7.14 Hz oscillation frequency for case 5, however, generates lower amplitude harmonics, and the effects of these are not easily seen in the response. Aside from the peak behavior associated with the driving frequency, the oscillation frequency appears to affect the width of the resonant response such that the higher the oscillation frequency, the sharper the resonant response. The sharpest resonant peaks, associated with load case 7, also appear to be at lower frequencies and generally higher amplitudes, than the resonant peaks for load case 6 and, to a greater extent, than those for load case 5.

The POD/modal expansion analysis identified 25 NMs associated with 20 POMs for load case 5, 24 NMs associated with 19 POMs for load case 6, and 28 NMs associated with 23 POMs for load case 7. The number of POMs of each type does not significantly differ, as shown in Table 4. Again, there is significant commonality between the corresponding set of NMs seen in Table 3.

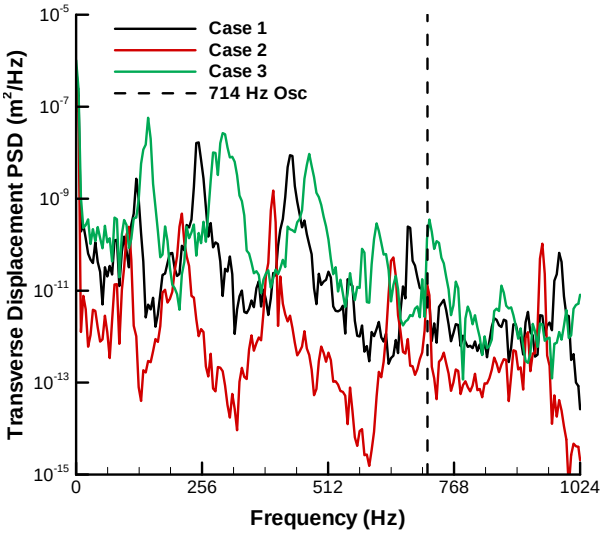

Figure 7: Effect of oscillation center position on the quarter-span transverse displacement PSD.

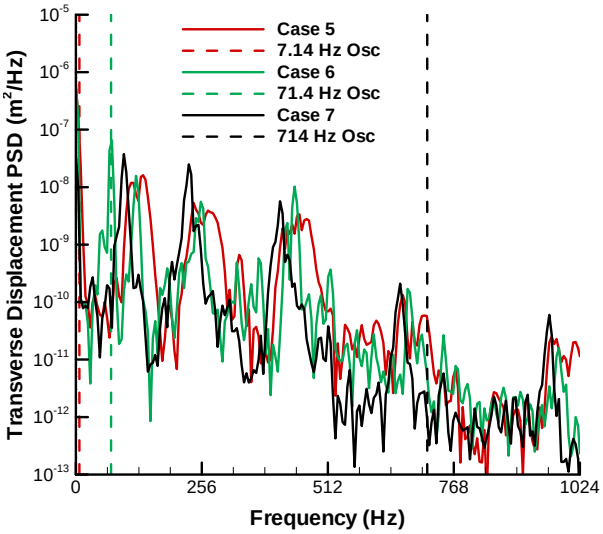

Figure 8: Effect of oscillation frequency on the quarter-span transverse displacement PSD.

Effect of Oscillation Span

Last, the effect of oscillation span was explored by perturbing load case 1 such that the span increased by a factor of 5 to 0.0635 m (load case 4) and by a factor of 10 to 0.127 m (load case 6), while maintaining the oscillation center position at the quarter-span and maximum oscillation speed of 28.49 m/s. Because the oscillation speed was maintained, the oscillation frequency was reduced from 714 Hz for load case 1, to 142.8 Hz for load case 4, and to 71.4 Hz for load case 6. Therefore, this perturbation was not independent of a change in frequency.

The quarter-span transverse displacement PSDs are shown in Figure 9. Here, both the 71.4 Hz and the 142.8 Hz oscillation frequencies significantly drive the responses of load cases 6 and 4, respectively. The POD/modal expansion analysis identified 25 NMs associated with 21 POMs for load case 4 and 24 NMs associated with 19 POMs for load case 6. The number of POMs of each type does not significantly differ between load cases 4 and 6, as seen in Table 4. Again, there is significant commonality between the corresponding NMs seen in Table 3.

E. Computational effort for individual and combined modal bases

If the seven loading conditions were considered individually, a separate reduced-order system would need to be formed for each using the modal bases presented in Table 3. Since cases 4 and 5 resulted in the same basis selection, only a single common reduced-order system need be formed for them. The computational effort associated with obtaining the reduced-order system for the resulting six bases can be computed per Eq. (15). The number of static nonlinear cases to be solved for each is presented in Figure 10 with the blue points. The total effort requires the solution of 24,606 static nonlinear cases.

In previous work, the authors demonstrated that expanding the modal basis does not adversely affect the quality of the reduced-order solution.[3] Because of this, only a single reduced-order system need be formed with a basis consisting of a superset of all modes identified in Table 3. As a result, a reduced-order system with 35 modal basis functions can be obtained and applied for the analysis of any or all of the cases under consideration. The cost associated with forming such a system requires the solution of 8,435 nonlinear static cases, as indicated with the black point in Figure 10. Consequently, the computational effort of modal reduction using a single combined basis is reduced by the factor of 2.92 relative to that of six individual reductions. Note that extent of perturbations from the baseline condition affects the number of common NMs between cases, and hence the efficiency to be gained by forming a common basis. For the seven cases considered in this work, 21 out of 35 NMs listed in Table 3 are common.

There are obstacles to using the POMs to form a combined modal basis. First, each set of POMs is load case specific. Therefore, a common basis would consist of all 151 POMs identified in Table 4 and would require the solution of 596,903 nonlinear static cases! Secondly, a basis formed in this manner would be comprised of vectors that are generally not orthogonal. This has been shown to lead to difficulties in integrating the reduced order system.[15]

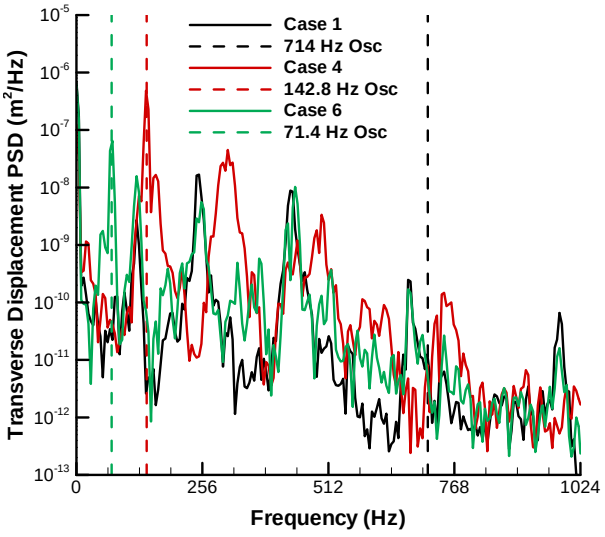

Figure 9: Effect of oscillation span on the quarter-span transverse displacement PSD.

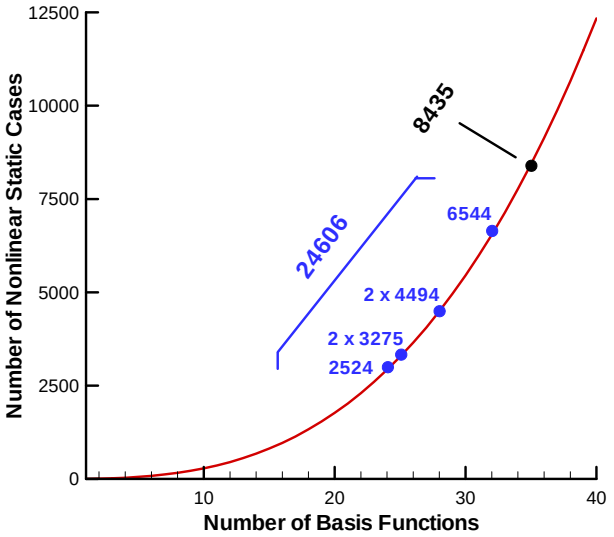

Figure 10: Computation cost associated with individual and combined modal bases.

IV. Conclusions

A nonlinear reduced-order modal simulation has been demonstrated to accurately predict the response of structures with time-varying spatial loading distributions provided that an appropriate modal basis is selected. Selection of such a basis requires knowledge of the system dynamics that can be gained by a system identification procedure. The proper orthogonal decomposition used for this purpose leads to a set of proper orthogonal modes, and while these may be used directly to form a reduced-order system, such a system is load specific. A load independent basis, however, is more desirable as it permits analysis of a broader range of loading conditions using the same reduced order system.

A load independent basis can be formed using normal modes which are identified via modal expansion of the proper orthogonal modes. By perturbing the baseline loading condition, the POD analysis and modal expansion can be repeated to incrementally expand the modal basis. The resulting basis was demonstrated to be more computationally efficient compared to independent analyses of all perturbed conditions.

References

[1]Hollkamp, J.J., Gordon, R.W., and Spottswood, S.M., "Nonlinear modal models for sonic fatigue response prediction: a comparison of methods," *Journal of Sound and Vibration*, Vol. 284, No. 3-5, 2005, pp. 1145-1163.

[2]Przekop, A. and Rizzi, S.A., "Efficient modal basis selection criteria for reduced-order nonlinear simulation," *EURODYN 2008, 7th European Conference on Structural Dynamics*, Paper E69, Southampton, UK, 2008.

[3]Rizzi, S.A. and Przekop, A., "System identification-guided basis selection for reduced-order nonlinear response analysis," *To appear in Journal of Sound and Vibration*, 2008.

[4]Feeny, B.F., "On proper orthogonal co-ordinates as indicators of modal activity," *Journal of Sound and Vibration*, Vol. 255, No. 5, 2002, pp. 805-817.

[5]Feeny, B.F. and Kappagantu, R., "On the physical interpretation of proper orthogonal modes in vibrations," *Journal of Sound and Vibration*, Vol. 211, No. 4, 1998, pp. 607-616.

[6]Blevins, R.D., Bofilios, D., Holehouse, I., Hwa, V.W., Tratt, M.D., Laganelli, A.L., Pozefsky, P., Pierucci, M., "Thermo-Vibro-Acoustic Loads and Fatigue of Hypersonic Flight Vehicle Structure - Phase II Report," ROHR Industries, Inc. RHR 89-202, Chula Vista, CA 1989.

[7]Dolling, D.S. and Murphy, M.T., "Unsteadiness of the separation shock wave structure in a supersonic compression ramp flowfield," *AIAA Journal*, Vol. 21, No. 12, 1983, pp. 1628-1634.

[8]Elfstrom, G.M., "Turbulent hypersonic flow at a wedge-compression corner," *Journal of Fluid Mechanics*, Vol. 63, No. 1, 1972, pp. 113-127.

[9]Muravyov, A.A. and Rizzi, S.A., "Determination of nonlinear stiffness with application to random vibration of geometrically nonlinear structures," *Computers and Structures*, Vol. 81, No. 15, 2003, pp. 1513-1523.

[10]Rizzi, S.A. and Przekop, A., "Estimation of sonic fatigue by reduced-order finite element based analyses," *Structural Dynamics: Recent Advances, Proceedings of the 9th International Conference*, Southampton, UK, 2006, M.J. Brennan, et al. (ed.).

[11]Allemang, R.J. and Brown, D.L., "A correlation coefficient for modal vector analysis," *Proceedings of International Modal Conference*, 1982, pp. 110-116.

[12]Doyle, J.F., Static and dynamic analysis of structures with an emphasis on mechanics and computer matrix methods, ed. G.M.L. Gladwell. Vol. Kluwer Academic Publishers, Dordrecht, The Netherlands, 1991.

[13]"ABAQUS version 6.6 on-line documentation, ABAQUS analysis user's manual," Abaqus, Inc., 2005.

[14]"MSC.NASTRAN 2005 quick reference guide," MSC.Software Corporation, 2004.

[15]Rizzi, S.A. and Przekop, A., "The effect of basis selection on static and random response prediction using nonlinear modal simulation," NASA TP-2005-213943, December 2005.